ADVANCED ENERGY MATERIALS
www.advenergymat.de

Single-Solvent-Based Electrolyte Enabling a High-Voltage Lithium-Metal Battery with Long Cycle Life

Yuanqin Li, Mingzhu Liu, Kang Wang, Chengfeng Li, Ying Lu, Aditya Choudhary, Taylor Ottley, Dmitry Bedrov, Lidan Xing,* and Weishan Li**

The application of Li-metal-anodes (LMA) can significantly improve the energy density of state-of-the-art lithium ion batteries. Lots of new electrolyte systems have been developed to form a stable solid electrolyte interphase (SEI) films, thereby achieving long-term cycle stability of LMA. Unfortunately, the common problem faced by these electrolytes is poor oxidation stability, which rarely supports the cycling of high-voltage Li-metal batteries (LMBs). In this work, a new single-component solvent dimethoxy(methyl)(3,3,3-trifluoropropyl) silane is proposed. The electrolyte composed of this solvent and 3 M LiFSI salt successfully supports the long-term cycle stability of limited-Li (50 µm)||high loading $LiCoO_2$ (≈20 mg cm^{-2}) cell at 4.6 V. Experiments and theoretical research results show that the outstanding performance of the electrolyte in high-voltage LMBs is mainly attributed to its unique solvation structures and its great ability to build a highly stable and robust interphase on the surface of LMA and high-voltage cathodes. Interestingly, this proposed electrolyte system builds a stable SEI film rich in LiF and Li_3N on the surface of LMA by improving the two-electron reduction activity of FSI^- without adding $LiNO_3$, the well-known additive used for LMBs. The design idea of the proposed electrolyte can guide the development of high-voltage LMBs.

1. Introduction

Among all anode materials of Li-ion batteries (LIBs), Li-metal anode (LMA) has the highest specific capacity (3862 mAh g^{-1}) and the lowest lithiation potential (−3.040 V relative to SHE).[1–6] And yet, the LMA, which was initially discarded in early LIBs and now is attracting renewed attention, still faces the problem of its highly reactive interface. The continuous reduction of electrolyte on the LMA surface and the formation of Li dendrites from the uneven deposition of lithium eventually bring on the low coulomb efficiency and great security risks of lithium-metal batteries (LMBs).[7–13] Li-metal structural modifications, surface treatments and adjustment of electrolyte formulations can restrain the above side reactions, improve cycle life and safety performance of LMBs to some extent.[7,14–23] Traditional carbonate-based electrolytes have been widely applied in LIBs for their excellent comprehensive performance.[24–26] Unfortunately, the carbonate-based electrolytes with conventional salt concentration (≈1 M) fail to form a stable solid electrolyte interphase (SEI) on the LMA surface. Increasing the concentration of salt can enhance the stability of SEI film formed by electrolyte, albeit at the expense of electrolyte conductivity and viscosity.[27] Ether-based electrolytes, in combination with appropriate film-forming additives such as $LiNO_3$, can facilitate the formation of a more robust solid-electrolyte interphase (SEI) on the surface of lithium metal. This approach greatly enhances the interphasial stability of lithium metal compared to carbonate-based electrolytes. However, application of such electrolytes faces the problems of low flash point and low oxidation stability.[22032] Phosphonate-based electrolytes with high salt concentration exhibit non-flammability and excellent SEI formation on Li-metal surfaces. However, their poor oxidation stability limits the long cycle life of high-voltage LMBs.[24] In our previous work, incombustible vinylethylene carbonate (VEC) was used as single solvent to construct an electrolyte system to ameliorate the cycling reversibility and safety of LMBs.[7] While the VEC-based electrolyte also failed to withstand at high voltage.

According to the above reported literatures, it is evident that new electrolyte systems capable of forming stable SEI films on Li-metal surfaces are not uncommon. However, most of these systems suffer from incompatibility with high-voltage cathode materials, which severely hinders the development and application of high-energy-density LMBs.[1322] The development of

Y. Li, M. Liu, K. Wang, C. Li, Y. Lu, L. Xing, W. Li
Engineering Research Center of MTEES (Ministry of Education)
Research Center of BMET (Guangdong Province)
Engineering Lab. of OFMHEB(Guangdong Province)
Key Laboratory of ETESPG (GHEI)
and Innovative Platform for ITBMD (Guangzhou Municipality)
School of Chemistry
South China Normal University
Guangzhou 510006, China
E-mail: xingld@scnu.edu.cn; liwsh@scnu.edu.cn
A. Choudhary, T. Ottley, D. Bedrov
Department of Materials Science and Engineering
University of Utah
122 South Central Campus Drive, Salt Lake City, UT 84112, USA
E-mail: d.bedrov@utah.edu.cn
The ORCID identification number(s) for the author(s) of this article can be found under https://doi.org/10.1002/aenm.202300918

DOI: 10.1002/aenm.202300918

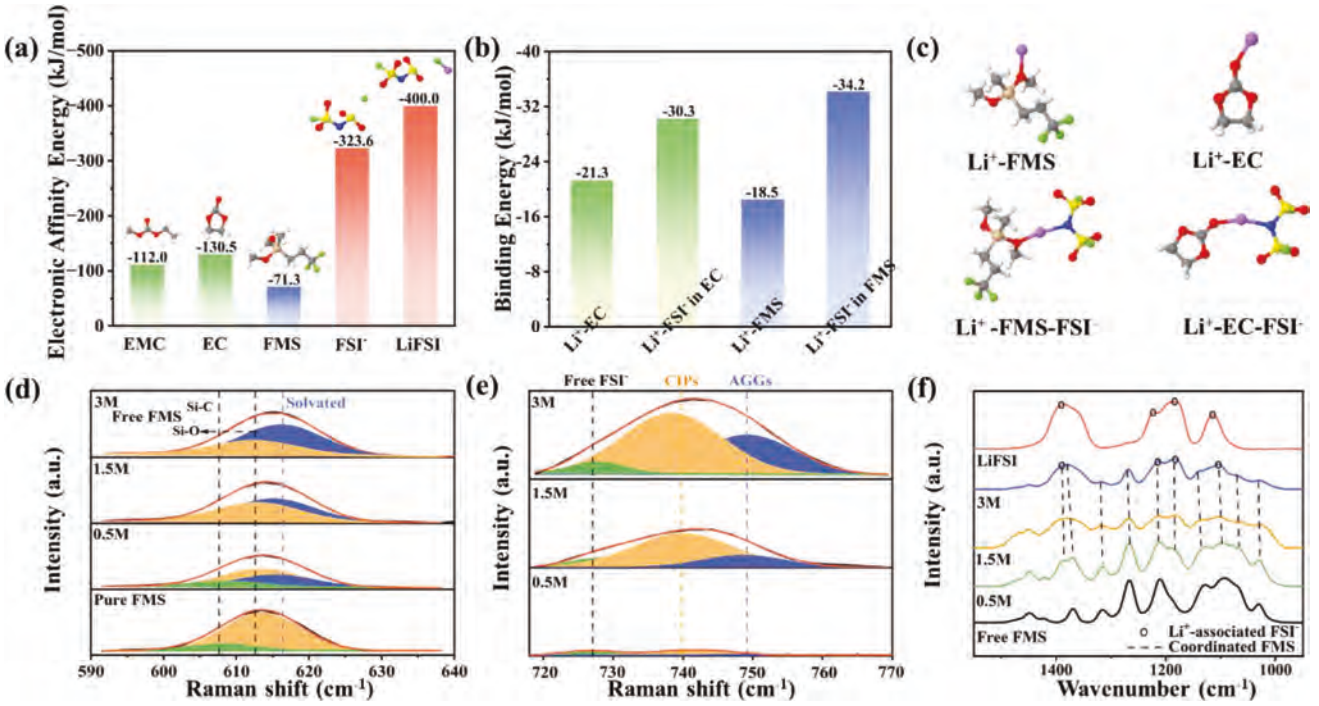

Figure 1. a) DFT-optimized structures and electronic affinity energy of the FMS, EC, EMC, LiFSI, and FSI^-. b)The binding energies between Li^+ and various species calculated by DFT. c) The optimized configurations between Li^+ and solvents/anions. The hydrogen, lithium, carbon, nitrogen, oxygen, fluorine, and sulfur atoms are represented by white, purple, grey, blue, red, green, and yellow, respectively. Raman spectra of siloxane electrolytes with different concentrations in the range of d) 590–640 cm^{-1} and e) 720–770 cm^{-1}. f) FTIR spectra of free LiFSI and siloxane electrolytes with different concentrations.

new electrolyte system with excellent film-formation capability on Li-metal and high interphasial stability at high voltage is of paramount importance.[33–36]

Fluorination can improve the reduction activity of the molecule, which is beneficial to its film-forming reaction at the anode side. In addition, the Si–O bond exhibits higher antioxidant stability compared to the C–O bond. Its presence can enhance the stability of the interphase formed at high voltage cathodes.[4,5] Based on these arguments, we investigate the possibility of using a fluorosilicone solvent, dimethoxy(methyl)(3,3,3-trifluoropropyl)silane (FMS; Figure S1a, Supporting Information) as a single-solvent electrolyte for the high-voltage LMBs. The results show that the binding energy between FMS solvent and Li^+ is relatively weak, which makes it easier to form Li^+-FSI^- ion contact solvation structure and larger aggregate structures (AGG, where one Li^+ binds two/or more FSI^- at the same time). These unique solvation characteristics are beneficial to the formation of an SEI film rich in anion decomposition product LiF on the Li anode. Moreover, FMS solvent can promote the complete decomposition of FSI^- ions and generate Li_3N and Li_2SO_3 redox reaction products. The resulting SEI film effectively inhibits the development of Li dendrites and improves the long-cycle Coulombic efficiency of Li//Li and Li//Cu cells. More importantly, FMS has excellent cathode film-forming ability. It takes precedence over FSI^- in oxidative decomposition, and forms a stable and robust cathode electrolyte interphase (CEI) film on the surface of 4.6 V lithium cobalt oxide (LCO) electrode, which significantly improves the high voltage interphasial stability. We demonstrate, that based on the unique solvation structure and outstanding film-forming performance of 3 M FMS-based electrolyte, the capacity retention of 4.6 V Li (50 μm)//high loading LCO (20 mg cm^{-2}) cell reached 92.5% after 100 cycles with the average Coulombic efficiency of 99.5%.

2. Results and Discussions

2.1. Compatibility of FMS-Based Electrolyte with LMA

The compatibility between the electrolyte and LMA is typically dependent on the properties of the SEI film formed by the electrolyte on the surface of lithium metal. The SEI film primarily comprises reduction products of electrolyte components with high reduction activity. Therefore, assessing the reduction activity of each component in the electrolyte is beneficial for predicting both the film-forming ability of the electrolyte and properties of the resulting SEI film. **Figure 1**a presents the calculated electronic affinity energy of EMC, EC, FMS solvents and FSI^- anion, together with LiFSI. The less negative electronic affinity energy of FMS compared to carbonate solvents indicates a lower reduction activity and probability of participating in reduction and decomposition into SEI products. In addition, the reducing activity of LiFSI can be found to be much superior to that of the studied solvent molecules. The reduction and decomposition of LiFSI will form an effective SEI component LiF. This shows that if the electrolyte forms a Li^+ solvation shell with ion contact, such as high salt electrolyte or local concentrated electrolyte, it is beneficial for building a stable SEI film rich in LiF on the anode surface.[37–49] The binding energies and structure of EC and FMS solvents with

Li^+ and Li^+ with FSI^- anions in these two solvents are compared in Figure 1b,c. The binding energy between Li^+ and FMS solvent (−18.5 kJ mol^{-1}) is weaker than that with EC. This makes the binding energy of Li^+-FSI^- in FMS solvent stronger than that of EC solvent, which is beneficial to the formation of ion contact solvation structures and AGG structures, and then to the formation of SEI film rich in LiF. These DFT calculation results show that, compared with EC-based electrolyte, FMS-based electrolyte is beneficial to promote the formation of ion contact solvation structures, and the reduction activity of FMS is low, which is helpful to form an efficient and stable SEI film with LiF as the main component on LMA.

Experiments were conducted to validate the aforementioned theoretical insight. 1 M LiFSI FMS electrolyte was tested in a Li//Cu cell (Figure S1b, Supporting Information) to check the electrochemical compatibility and reversibility of FMS with Li metals. Surprisingly, even though the salt concentration in the electrolyte is only 1 M, FMS-based electrolyte exhibited an average Coulombic efficiency (CE) up to 98.4%. Moreover, the average CE of Li//Cu cell in FMS-based electrolyte is obviously higher than that of EC/EMC-based electrolyte (Figure S1c, Supporting Information). Figure S2 (Supporting Information) shows that the wettability of FMS-based electrolytes with the separator is better than that of EC/EMC-based electrolytes. From the data of Figure S3a (Supporting Information), it can be seen that the conductivity of FMS-based electrolytes is lower than that of carbonate-based ones. This suggests that the higher average CE of FMS-based electrolyte is primarily attributed to its enhancement of the interphasial stability of Li metal, which aligns with the capability of FMS-based electrolyte to facilitate more LiFSI involvement in reduction and decomposition compared to carbonate-based electrolyte (CBE) at 1 M salt concentration, thereby generating a more robust interphase. More importantly, as shown in the Figure S1c (Supporting Information), the CE data are even better than that of other reported electrolytes for LMA, including tetrahydrofuran (THF), dimethoxyethane (DME), 1,4-dioxane (1,4-DX) and 2-methyltetrahydrofuran (MeTHF), and is equivalent to that of 2,5-dimethyltetrahydrofuran (DMeTHF).[41] The viscosity of pure solvents and each electrolyte systems are shown in Figure S3b (Supporting Information).

In general, increasing the salt concentration in the electrolyte can further increase the content of ion contract solvation shells, thus improving the performance of SEI constructed at the anode surface.[22] The FMS-based electrolyte is no exception. As shown in Figure 1d, the pure FMS solvent exhibits a vibration peak attributed to Si–O at 613 cm^{-1}. When it combines with Li^+, the peak shifts to 617 cm^{-1}, and its proportion increases with the increase of LiFSI concentration. At the same time, Li^+-FSI^- binding is enhanced through the formation of contact ion pairs (CIPs) and cation–anion aggregates (AGGs) as reflected by the FSI^- band (720–770 cm^{-1}; Figure 1e) rises significantly. At lower LiFSI concentration (0.5 M), free FSI^- contributes about 36.5%, while the remaining anions are participating in CIPs and AGGs. As the LiFSI concentration increases from 0.5 to 3.0 M, the proportion of free FSI^- anions drops to 6%–7% and majority of the anions are in clusters (Table S1, Supporting Information). The aggregation of LiFSI in FMS systems could be further disclosed by a band complex in the range of 900–1500 cm^{-1}, whereas the shift of the Li^+-associated FSI^- bands toward those at 1122, 1170, 1226, and 1360 cm^{-1} for $\nu_{s,SO2}$ or $\nu_{as,SO2}$ vibrations of pure LiFSI shows the gradually strengthened Li^+-FSI^- association, and ν_{Si-O}(1020, 1080, 1130cm^{-1}), ν_{Si-C}(1260, 1410cm^{-1}), ν_{Si-C}(1325cm^{-1}) and $\delta_{s,CH3}$ (1374 cm^{-1}) of FMS on the same spectra confirms their coordination in the 3 M electrolyte. FTIR results are in accord with the Raman results. The peak intensity of pure FMS solvent gradually weakens with the increase of salt concentration, and the peak position undergoes a certain "red-shift," indicating that the fraction of free FMS solvent decreases and more participates in the Li^+ solvation sheath.

Atomistic molecular dynamics (MD) simulations employing polarizable force field (SI for simulation details) provide additional molecular scale insight into electrolyte structure and dynamics. It is instructive to compare properties of FMS-based electrolytes with the reference EC/EMC-based electrolytes. Simulations were conducted for pure FMS and EC/EMC solvent systems as well as for 1, 2, and 3 M LiFSI compositions at 298K. **Figure 2**a shows representative snapshots from 1 and 3 M systems, highlighting distribution of ions. As expected in 1 and 3 M EC/EMC electrolytes, Li^+ and FSI^- ions are homogeneously distributed through the system. Analysis of radial distribution functions shows a strong preference of O atoms from the solvent(O_{FMS}, O_{EC}, and O_{EMC}) and FSI^- (O_F) to comprise the first coordination shell of Li^+ that can be defined as a sphere of 2.9 Å around the cation (Figure 2b). Due to strong interaction between carbonate solvents and Li^+ the LiFSI salt is well dissociated in the EC/EMC electrolytes and cation is primarily coordinated with EC and EMC oxygen atoms (Figure 2b). As the salt concentration increases the amount of FSI^- oxygen atoms in the 1st coordination shell of Li^+ growth from about 0.3 to about 1.0, which is compensated by similar reduction of O atoms from EMC, while the number of O atoms of EC stays basically the same around 2.0. A qualitatively different structure is observed in the FMS-based electrolytes. Figure 2a shows that majority of ions are aggregated, which is in good accordance with the Raman results. At 1 M the salt forms large ionic clusters, but the clusters are not percolating. At 3 M concentration, the formed LiFSI domains are continuous and the formation of percolating nanosegregated salt domains is observed, which is consistent with mentioned above Raman data. Li^+ coordination is also different for these electrolytes and is primarily dominated by the O atoms from FSI^- with less than one oxygen contributed by FMS solvent.

It is also instructive to analyze dynamical properties of electrolytes. Figure 2c shows the self-diffusion coefficients of solvent molecules obtained from MD simulations at different salt concentrations including pure solvents. FMS systems show a noticeably larger diffusivity of FMS compared to carbonates, which is consistent with the lower viscosity of this solvent compared to EC-EMC mixture (Figure S3b, Supporting Information). However, ion diffusivity in FMS-based solvents is significantly lower (almost an order of magnitude) compared to that in the carbonate-based systems, which is consistent with the observed aggregation of the salt in FMS solvent which weakly interacts with Li^+ (as demonstrated by DFT calculations). Therefore, the ionic conductivity of FMS-based electrolytes, shown in Figure 2d, is about an order of magnitude lower compared to that in EC-EMC solvents. The conductivity predicted by the simulation fitted well with the experimental data (Figure S3a, Supporting Information) and also capture the increase of conductivity in FMS systems with

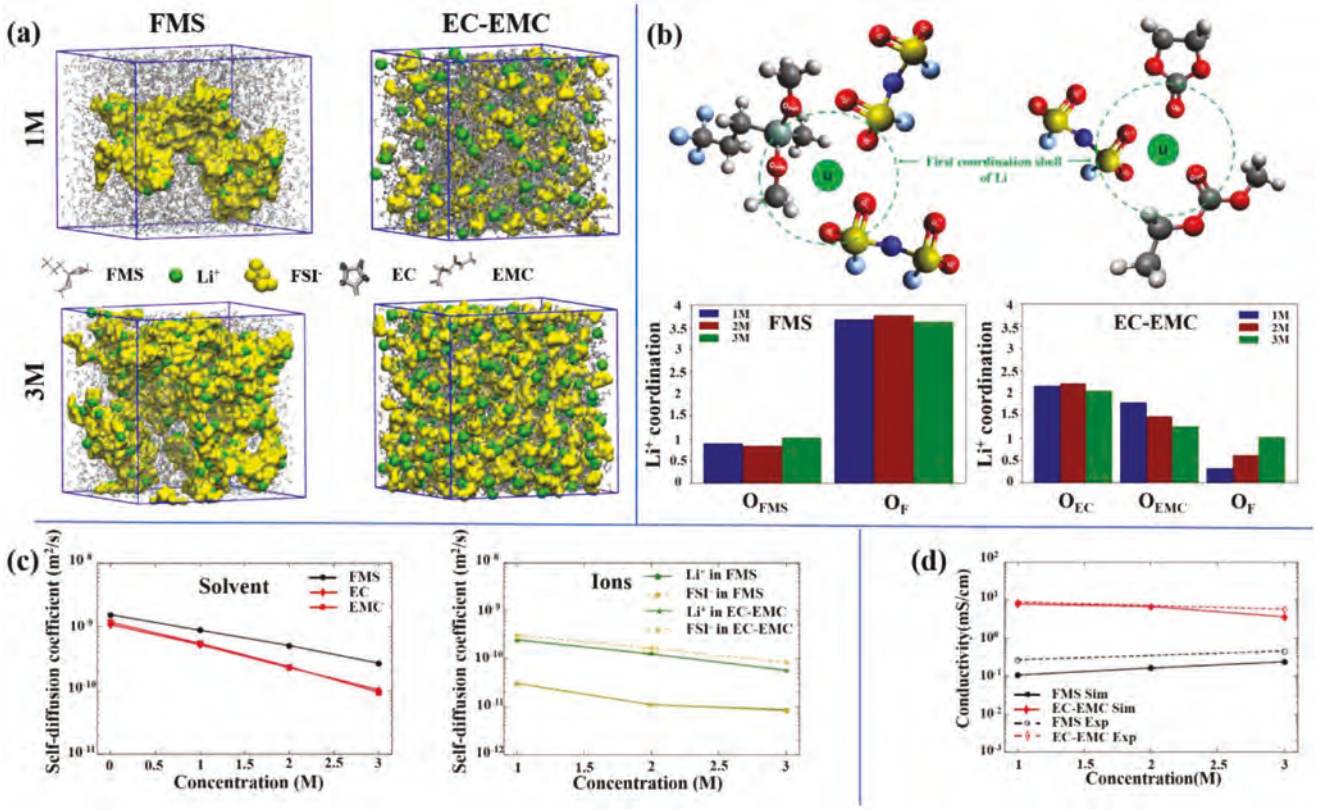

Figure 2. a) Snapshots from MD simulations of FMS (left column) and EC/EMC (right column) based electrolytes with 1 and 3 M LiFSI concentrations. Solvent molecules are shown using wireframe representation, while Li^+ and FSI^- ions are highlighted in green and yellow, respectively. b) Schematic illustration of the definition of the 1st coordination shell of Li^+ (a sphere of 2.9 Å radius) and the number of O atoms of different types in the 1st coordination shell for FMS and EC-EMC electrolytes as a function of salt concentration. c) Self-diffusion coefficients of solvent molecules (left panel) and ions (right panel) as a function of salt concentration. d) Ionic conductivity of electrolytes as a function of salt concentration obtained from MD simulations and from experiments.

increasing LiFSI concentration. As we discussed above and will demonstrate below, although the ionic conductivity of FMS-based electrolyte is not as good as that of CBE due to more salt aggregate structures, especially at a salt concentration of 3 M, the observed salt aggregates are beneficial to the construction of a more stable SEI film on the surface of Li metal.

2.2. Highly Reversible Li Depositing/Stripping

The deposition behavior of Li with 1 M EC/EMC-based, 3 M EC/EMC-based and 3 M FMS-based electrolytes on Cu substrates was investigated. As depicted in Figure S4a,d (Supporting Information), the initial deposition of Li on a Cu substrate in the 1 M EC/EMC-based electrolyte results in the formation of acicular Li dendrites. These dendrites exhibit high permeability to the separator, which can lead to internal short circuits or catastrophic thermal runaway failure within the cell. This instability is a major safety concern for LMBs. When Li was deposited on the Cu substrate in 3 M EC/EMC-based electrolyte (Figure S4b,e, Supporting Information), dendritic metallic Li is obviously reduced, which is mainly due to the LiF-rich interphasial film formed on the surface of Cu substrate by high salt electrolyte, which is advantageous for improve the interfacial stability and the deposition of metallic lithium.[1–3] However, as depicted in Figure S4c,f (Supporting Information), the deposition of metallic lithium in 3 M FMS-based electrolyte is notably smoother compared to CBE. Furthermore, minimal formation of lithium dendrites suggests that FMS-based electrolyte exhibits superior interphasial properties with lithium metal under identical salt concentration.

The CE of Li//Cu cells during cycle at a current density of 1.0 mA cm^{-2} are presented in **Figure 3**a, which was calculated as the ratio of the amount of Li deposited on and stripped from Cu substrate. It can be seen that that the averaged CE of the cell with 1 M EC/EMC-based electrolyte is only 90.2% after 100 cycles, confirming the poor interphasial stability of Li with traditional CBE. Consistent with the morphological changes of metallic lithium shown in Figure S4 (Supporting Information), increasing the concentration of lithium salt in CBE can improve the interphasial stability of Li. The averaged CE of Li//Cu cell with 3 M EC/EMC-based electrolyte reaches 94.9% after 100 cycles. However, even so, the Li//Cu cell failed after around 150 cycles, which is likely due to the formation of a small amount of lithium dendrites in the system (Figure S4e, Supporting Information), leading to internal short circuit of the cell. In marked contrast, the Li//Cu cell with 3 M FMS-based electrolyte exhibits stable Li deposition/stripping reaction and remarkable cycling stability approach 500 cycles at 1 mAh cm^{-2}, with an averaged CE up to 99.1%.

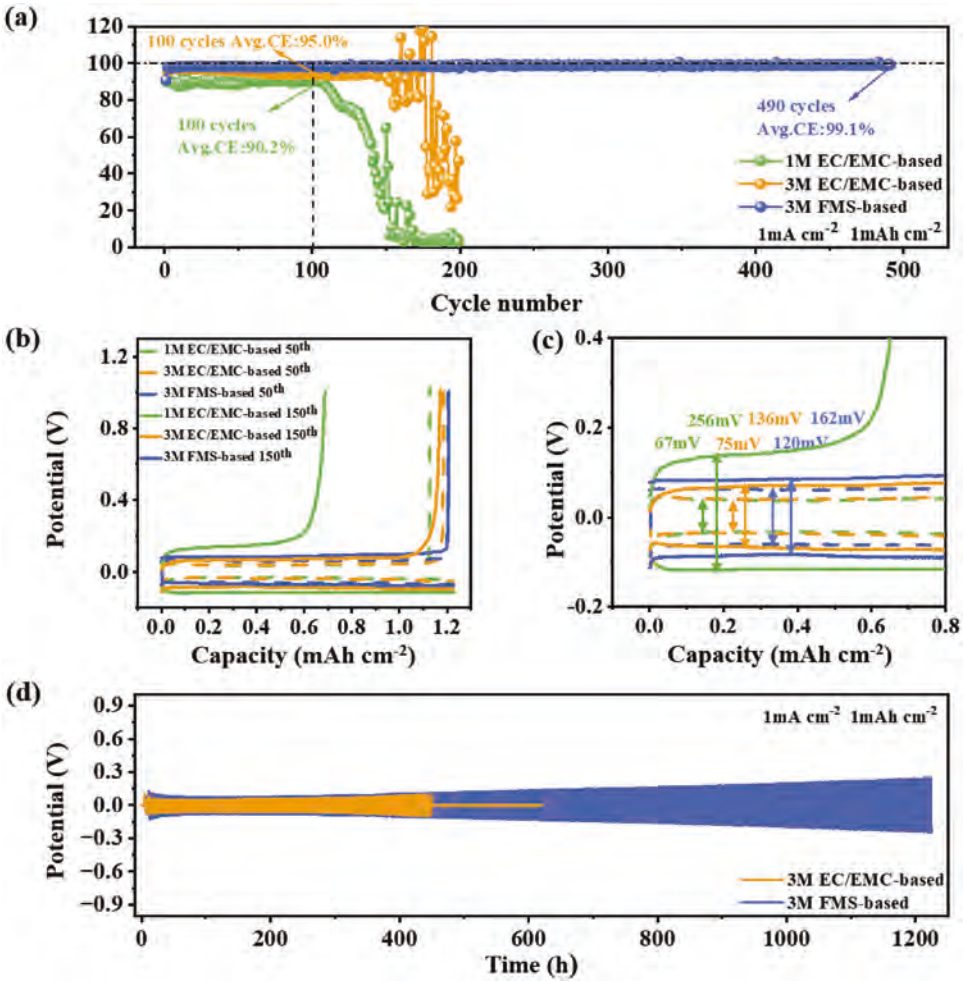

Figure 3. a) Average Coulombic efficiency in Li||Cu cells at current densities of 1.0 mA cm^{-2}. b,c) Polarization curves of plating/stripping process in Li||Cu cells. d) The voltage profiles in Li||Li symmetrical cells at current densities of 1.0 mA cm^{-2}.

Meanwhile, the selected polarization curves of Li//Cu cells also show that the 3 M FMS-based electrolyte shows higher interphasial stability (Figure 3b,c). In particular, during the 50th to 150th cycles, the polarization of Li deposition/stripping reaction increased by only 42 mV with the use of 3 M FMS-based system, whereas it increased by 61 mV with the use of 3 M EC/EMC-based system. The superior reversibility of Li deposition/stripping with FMS compared to CBE can be attributed to the distinctive interfacial morphology and chemistry resulting from the former electrolyte.

Figure 3d shows the voltage profiles of Li//Li symmetrical cells at a current density of 1.0 mA cm^{-2}. Similar to the findings of Li//Cu cells, the 3 M FMS-based system exhibits superior cycle stability, with only a slight increase in electrode polarization even after 1200 h of reaction. While the one with 3 M EC/EMC-based system experienced a short circuit after 420 h of operation. Moreover, even at a higher current density (2.0 mA cm^{-2}), the Li//Li and Li//Cu cells with 3 M FMS-based electrolyte still shows the best cycle stability and the highest CE (Figure S5, Supporting Information). As depicted in Figure S6 (Supporting Information), the superior rate performance of Li//Li and Li//Cu cells cycled in 3 M FMS-based electrolyte compared to that in 3 M carbonate-based electrolyte further implies that the former facilitates the formation of a stable SEI interface and uniform lithium deposition.

The evolution process of the deposition morphology of lithium ions on the metal lithium sheet is shown in Figure S7 (Supporting Information). Evidently, the initial deposition of lithium in 3 M carbonate-based electrolyte exhibits irregular and porous characteristics. This leads to a significant increase in the specific surface area of deposited lithium metal, resulting in subsequent electrode polarization as illustrated in Figure 3. Additionally, due to its rapid growth, the deposited lithium pierces the separator more quickly and contacts with the cathode material, resulting in an internal short circuit. While, the deposition of lithium in 3 M FMS-based electrolyte is uniform and dense, effectively inhibiting the growth of lithium dendrites and subsequent electrode polarization.

The results of Li deposition/stripping reaction and surface morphology above demonstrate that the SEI formed by 3 M FMS-based electrolyte can effectively suppress the growth of lithium dendrites, facilitate the reversibility of lithium deposition/stripping reaction, and enhance the cycle stability and high safety of LMA.

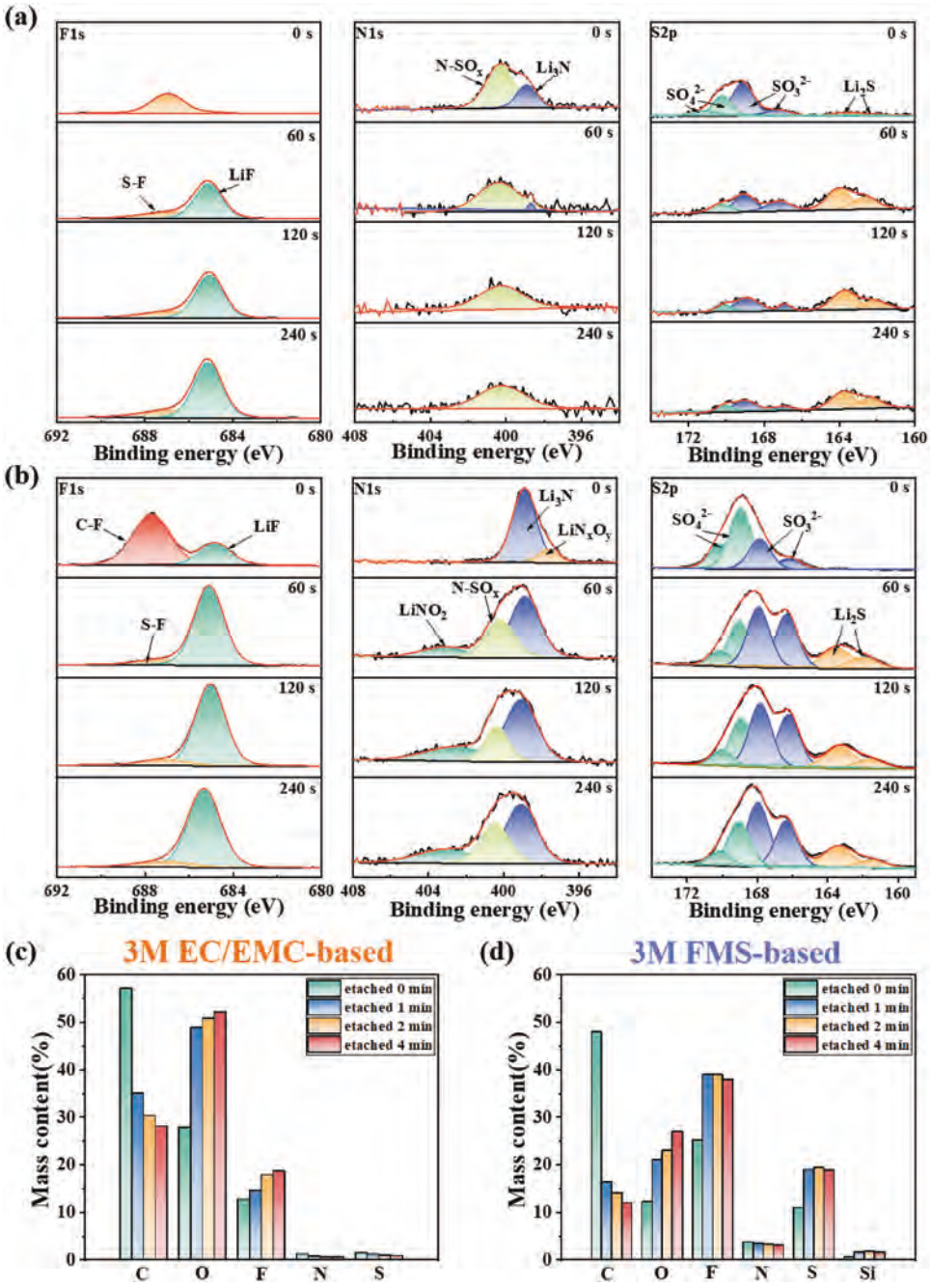

Figure 4. XPS survey spectra of lithium metal in different electrolytes at various argon (Ar^+) sputtering depths in the interphases on Li electrodes, collected by disassembling Li||Li cells after 10 cycles at a current density of 1 mA cm^{-2} with a capacity of 1 mA cm^{-2}. The XPS depth profiles of F 1s, N 1s, and S 2p in the 3 M EC/EMC-based electrolyte a) and 3 M FMS-based electrolyte b). Corresponding relative mass content from XPS spectra of Li electrodes cycled in 3 M EC/EMC-based electrolyte c) and 3 M FMS-based electrolyte d).

2.3. Key Components of the Constructed SEI and Its Formation Mechanism

The morphology and properties of the interphase film, which is a crucial factor affecting cell performance, are determined by the composition and structure of electrolyte reduction products. Therefore, X-ray photoelectron spectroscopy (XPS) was employed to investigate in detail the main components and their distribution within SEI films formed on lithium-metal surfaces using carbonate-based and FMS-based electrolytes, as illustrated in **Figure 4**.

The F1s spectrum data are in agreement with the aforementioned DFT and MD simulation results. In contrast to the carbonate-based system, a C-F peak (687.9 eV) was observed on the outermost layer of SEI film formed by the FMS system, which is attributed to the reduction decomposition of FMS. The results

indicate that FMS exhibits a lower reduction activity compared to LiFSI, and its reduction occurs only after the reduction of LiFSI, which is in agreement with the DFT calculations. The peak located at 684.8 eV is ascribed to the LiF component.[50–52] Compared to carbonate-based solvents, FMS solvent facilitates the formation of ion-contact and AGG structures, resulting in a higher LiF content in the SEI film constructed by FMS-based electrolyte at the same LiFSI concentration, particularly in the outermost layer of SEI film. Note that the CBE system contains a higher proportion of S-F (686.4 eV), which is also one of the main decomposition products of LiFSI,[42–54] compared to the FMS system. This may be attributed to the fact that in the FMS system, the F element in FSI^- primarily participates in forming LiF, resulting in less formation of S-F than its counterpart. These findings suggest that the FMS solvent not only facilitates the formation of a greater number of AGG structures in the electrolyte, but also enhances the extent of decomposition of FSI^-.

Importantly, the same conclusion can be obtained from the N1s and S2p spectrograms shown in Figure 4. In the N1s spectrum, the peaks observed at 397.4, 398.7, 400.2, and 403.2 eV correspond to LiN_xO_y, Li_3N, N-SO_x and $LiNO_2$ products respectively, which are generated through the decomposition of LiFSI.[10,55,56] The most conspicuous disparity in the N 1s spectrum between the two systems is that Li_3N generated by FMS-based electrolyte on lithium-metal surface exhibits a significantly higher intensity than that of carbonate system, and it is uniformly distributed throughout the entire SEI film akin to LiF. A plethora of prior research has demonstrated that the development of SEI films abundant in LiF and Li_3N on the surface of lithium metal can significantly enhance the stability of the interface of lithium metal.[57–60] Therefore, the presence of higher amounts of LiF and Li_3N in the SEI film may serve as a fundamental factor contributing to the superior performance of FMS-based electrolyte on lithium-metal anode compared to carbonates. In the aforementioned references, Li_3N was generated through the addition of $LiNO_3$ as a film-forming additive. In contrast, our study employed FMS solvent to facilitate the formation of an interphase rich in LiF and Li_3N from LiFSI salt. The S 2p spectrum results also indicate that the number of LiFSI involved in SEI film formation reaction is higher in FMS-based electrolyte than CBE system, leading to the generation of compounds such as Li_2S (159–165 eV), SO_3^{2-} and SO_4^{2-} (166–171 eV) which are uniformly distributed throughout the SEI film.[49,61] The HRTEM results presented in Figure S8 (Supporting Information), combined with the O1s spectrum shown in Figure S9 (Supporting Information), provide further evidence that the SEI formed by 3 M FMS-based electrolyte is abundant in LiF, Li_3N, Li_2SO_3 and Li_2SO_4.

Figure 4c, d illustrate the corresponding mass concentration of elements on the lithium surface at different etching times. Similarly, the results suggest that the SEI film formed by the 3 M FMS-based electrolyte system exhibits a higher concentration of F, N and S elements in comparison to the 3 M EC/EMC-based electrolyte system. Meanwhile, it displays relatively lower levels of C and O elements. This again indicates that the 3 M FMS-based electrolyte involves more FSI^- in SEI formation while the 3 M EC/EMC-based electrolyte has more solvent involved in SEI formation, which is consistent with solvation results.

The theoretical simulation results depicted in Figures 1 and 2 demonstrate that the utilization of FMS solvent is conducive to promoting the formation of more AGG structures within the electrolyte containing LiFSI, thereby enhancing its reduction activity and facilitating the development of an interphase rich in LiF. To understand the mechanism behind the ability of FMS to promote complete decomposition of LiFSI and enhance the concentration of crucial components such as Li_3N and Li_2SO_3 in the interface phase, we conducted further investigations into how solvent molecules influence the subsequent reduction and decomposition of LiFSI using DFT calculations. **Figure 5**a illustrates the electron affinity values and corresponding reduction products of LiFSI, EC-LiFSI, and FMS-LiFSI upon obtaining the first and second electrons. The corresponding optimized structures of reduction products are presented in Figure S10 (Supporting Information). The observation is in line with the computational findings depicted in Figure 1a, where LiFSI exhibits significantly higher reduction activity compared to EC and FMS solvents. Consequently, when electrons are transferred to EC-LiFSI and FMS-LiFSI systems, the reduction reaction takes place on LiFSI. Moreover, it is noteworthy that upon obtaining the second electron, the reduction activity of the FMS system (−553 kJ mol^{-1}) surpasses that of the EC system (−511 kJ mol^{-1}), indicating that FMS solvent indeed facilitates the reduction and decomposition of LiFSI. Of greater significance, following the two-electron reduction of LiFSI, all remaining products except for LiF will react with both Li^+ in electrolyte and residual Li_2CO_3 and Li_2O on electrode surface to form Li_2SO_3 and Li_3N. Thus far, it has been demonstrated that FMS enhances the reduction activity of LiFSI, particularly in terms of its second electron reduction capability. Consequently, the FMS system facilitates a more thorough decomposition of LiFSI, resulting in a SEI rich in Li_3N and Li_2SO_3 that enhances the interphasial stability of LMA.

2.4. Electrochemical Performance of Limited Li Anode with High Loading $LiCoO_2$ Cathode

For further investigation into the stability of the constructed SEI on lithium surface under high voltage conditions (up to 4.6 V) and limited lithium availability, we assembled and tested LMBs utilizing a high loading $LiCoO_2$ cathode (H-LCO) and a 50 μm thick lithium anode (L-Li). The superiority of 3 M FMS-based electrolyte in L-Li||H-LCO cells is more pronounced. As depicted in **Figure 6**a, the capacity of the 3 M carbonate-based system is nearly depleted after only ten cycles, whereas the capacity retention of the 3 M FMS-based system remains as high as 92.5% even after one hundred cycles with an average CE of 99.5% (Figure 6b). In contrast to the carbonate-based system, the discharge voltage plateau of the 3 M FMS-based system exhibits remarkable stability throughout the entire cycle, indicating excellent interphase formation durability (Figure 6c,d). Also, as can be seen from Figure 6c, the charging curve of the carbonate-based system shows an abrupt voltage drop during the 9th charging, which may be due to the uneven deposition of lithium causing a micro-short circuit. Importantly, even under more harsh conditions, high temperature (60 °C) and high voltage (4.6 V), the 3 M FMS-based system still shows excellent cycle stability. As shown in Figure 6e,f, after 50 cycles the capacity retention of the L-Li||H-LCO battery with 3 M FMS-based electrolyte is still as high as 86.7%. In stark contrast, the 3 M EC/EMC-based system

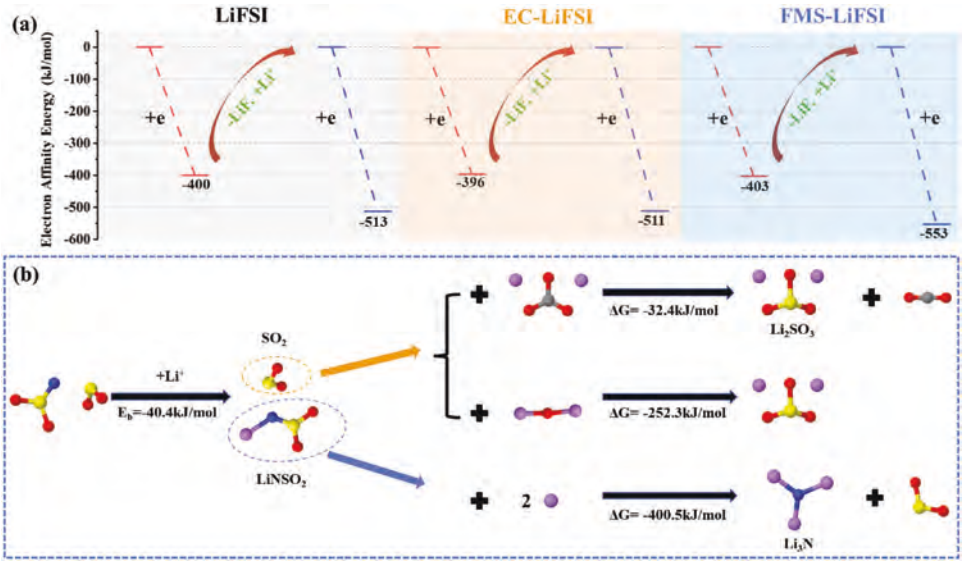

Figure 5. a) Possible reductive decomposition mechanism of LiFSI, Li^+-EC-FSI^- and Li^+-FMS-FSI^- together with the electron affinity energies (EAE, kJ mol^{-1}), b) possible reductive decomposition products of FSI^-–$2F^-$ of together with the reaction energy (kJ mol^{-1}).

showed a short circuit in 3 cycles and a very low Coulombic efficiency, indicating that the 3 M EC/EMC-based system decomposes very severely under high temperature conditions and has rapid lithium dendrite growth. The voltage profiles of Li//Li symmetrical cells and the CE for Li//Cu cells shown in Figure S11 (Supporting Information) further verify that the interphasial stability of metallic Li is better in the 3 M FMS-based electrolyte even at high temperature. It is worth noting that the polarization increase of Li//Li symmetrical cells in Figure S11 (Supporting Information) is more significant than that in Figure 3d, mainly due to increased electrolyte side reactions at high temperatures. The accumulation of decomposition products on the

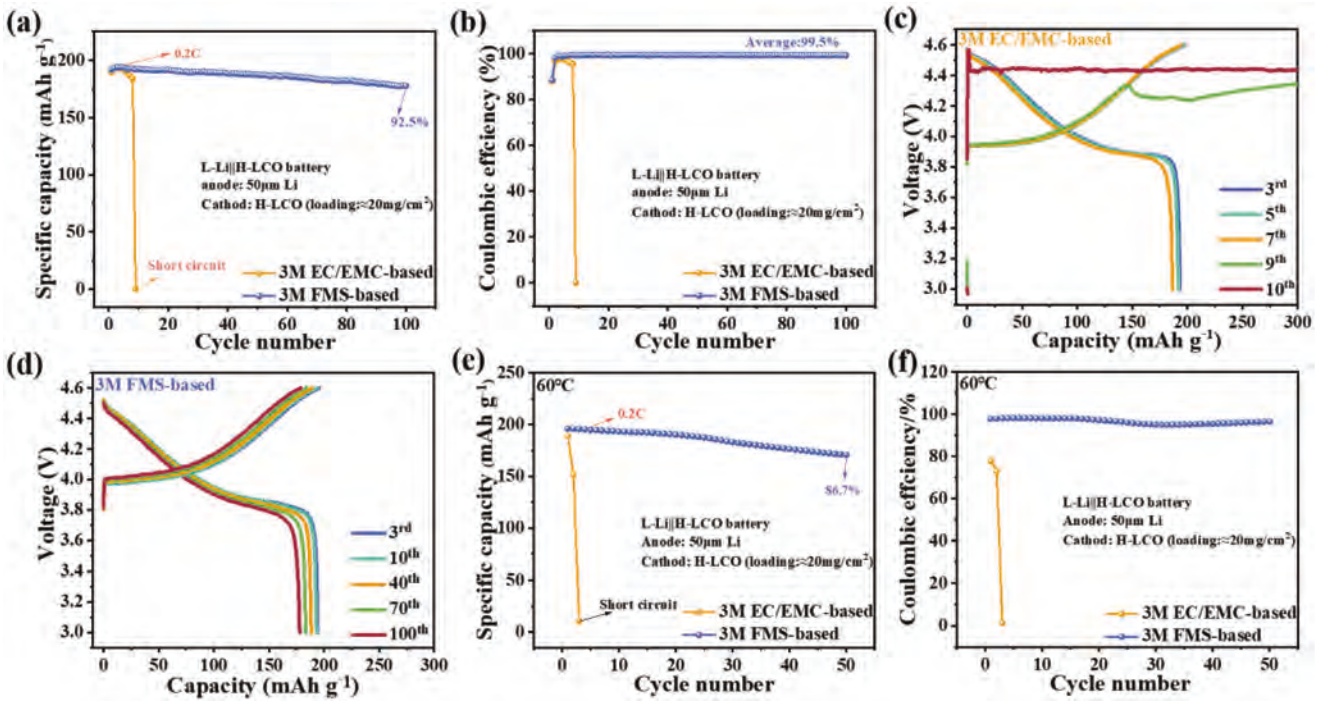

Figure 6. a) Cyclic stability and b) Coulombic efficiency of L-Li||H-LCO full batteries in different electrolytes at 0.2 C for all cycles between 3 and 4.6 V under room temperature. Selected charge–discharge curves of L-Li||H-LCO full batteries in 3 M EC/EMC-based electrolyte c) and 3 M FMS-based electrolyte d). e) Cyclic stability and f) Coulombic efficiency of L-Li||H-LCO full batteries were cycled at 0.2 C for all cycles between 3 and 4.6 V under 60 °C high temperature.

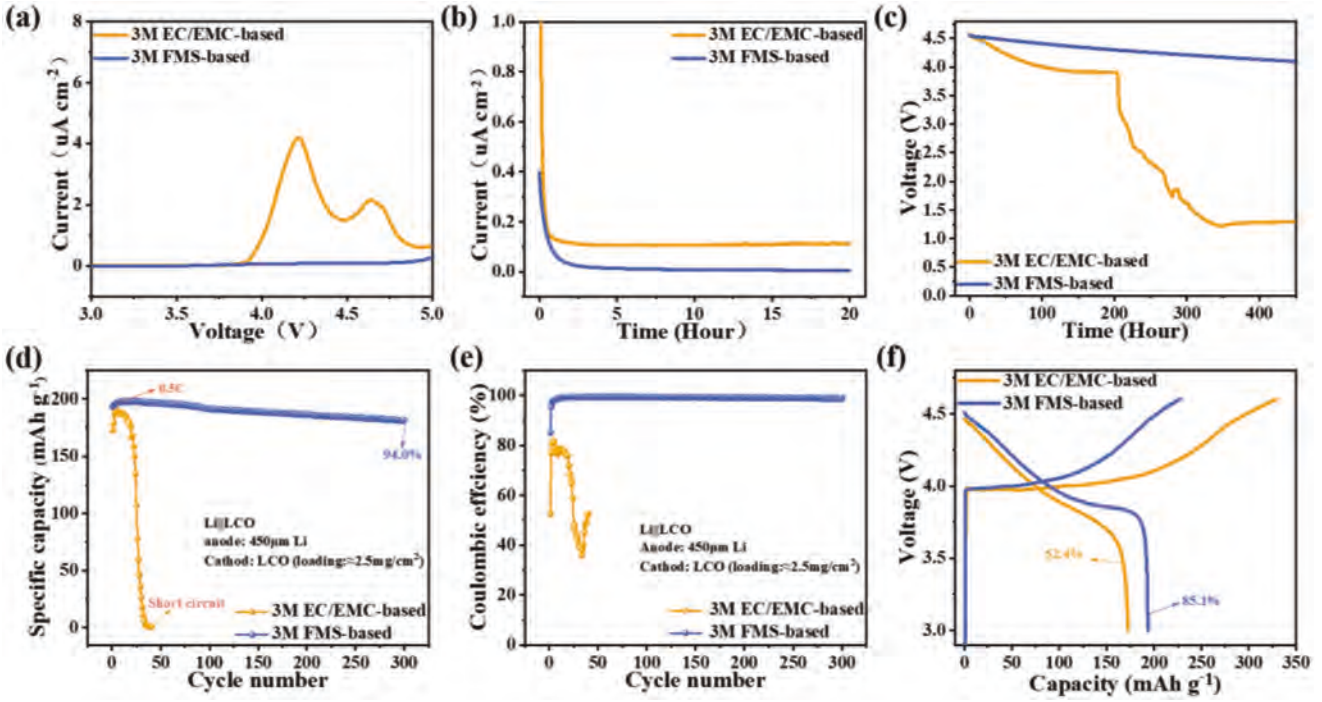

Figure 7. a) Linear sweep voltammograms of Li/Pt batteries in 3 M EC/EMC-based electrolyte and 3 M FMS-based electrolyte from 3 to 5 V at a scan rate of 0.1 mV s^{-1}. b) Chronoamperometric profiles for LCO||Li batteries at 4.6 V. c) Self-discharge profiles after three charge/discharge cycles for Li||LCO batteries in 3 M EC/EMC-based electrolyte and 3 M FMS-based electrolyte. d) Cyclic stability and e) Coulombic efficiency of Li||LCO batteries in different electrolytes. f) Initial charge/discharge profiles of Li||LCO batteries in different electrolytes at 0.5 C rate.

surface of lithium metal results in an impedance and polarization rise.

DME is a representative ether solvent used in lithium-metal systems.[27] For comparison, we prepared a 3 M LiFSI DME electrolyte for cycling tests in an L-Li||H-LCO battery. The results of this system are presented in Figure S12 (Supporting Information). After 40 cycles, the capacity retention of the 3 M LiFSI DME electrolyte in the L-Li||H-LCO battery was almost zero and its Coulombic efficiency was very low. This indicates that the 3 M LiFSI DME electrolyte also decomposes significantly at high voltage and cannot form a stable interphase.

It is noteworthy that despite the numerous reports on new electrolyte systems exhibiting high compatibility with Li metal,[1–23] only a few of them are capable of supporting the cycling of LMB at elevated voltage. Therefore, the exceptional performance of 3 M FMS-based electrolyte in ultrahigh voltage (4.6 V) L-Li||H-LCO batteries can also be attributed to its interfacial stability under high-voltage conditions. It is necessary to systematically study the interfacial stability of 3 M FMS-based electrolytes on the surface of high-voltage LCO cathode.

2.5. Interphasial Stability of FMS-Based Electrolyte with 4.6 V LCO Cathode

The LSV curves of electrolytes on the Pt electrode are presented in **Figure 7**a. It is observed that the oxidation current of 3 M EC/EMC-based electrolyte initiates at approximately 3.72 V, and its decomposition intensifies with an increase in electrode potential. Although the initial oxidation reaction of the 3 M FMS-based electrolyte occurs at a lower potential (3.55 V) than that of the carbonate-based system (Figure S13a, Supporting Information), its oxidative decomposition reaction effectively inhibits further electrolyte oxidation, demonstrating exceptional interfacial stability at high voltage. Indeed, as illustrated in Figure S13b (Supporting Information), among the investigated solvent systems, FMS exhibits the lowest ionization energy, indicating its high susceptibility to oxidative decomposition reactions. Nevertheless, the oxidative decomposition products of 3 M FMS-based electrolyte form a stable cathode electrolyte interface (CEI) film. It is important to note that the decomposition of electrolyte may result in the release of gas products, which could limit its practical application. To demonstrate the gas production of electrolyte, we conducted linear scanning and constant voltage holding tests on sealed V-type LCO/Li cells using 3 M EC/EMC-based (Figure S13c, Supporting Information) and 3 M FMS-based (Figure S13d, Supporting Information) electrolytes at a voltage of 4.6 V for 12 h. After cycling in the 3 M EC/EMC-based electrolyte, it is evident that the liquid level on the LCO cathode side decreases while the liquid level on the lithium electrode side rises, resulting in a significant difference between two liquid levels. This indicates that a certain amount of gas is generated on the cathode side. In sharp contrast, the liquid levels remained virtually unchanged before and after cycling in 3 M FMS-based electrolyte, indicating negligible gas generation during cycling. To further verify the occurrence of gas production, electrochemical mass spectrometry (DEMS) testing was also performed on the LCO/Li cell (Figure S13e, Supporting Information). The test results indicated

that the 3 M EC/EMC-based electrolyte exhibited a tendency to generate CO_2 during charging, whereas no gas evolution was observed for the 3 M FMS-based electrolyte. The results once again demonstrate that the utilization of FMS-based electrolyte significantly enhances the interphasial stability of the LCO cathode, effectively suppressing oxidation decomposition and gas generation at high voltages.

A large number of previous studies have demonstrated that increasing the content of the LMA (where Li undergoes "shallow" stripping) while reducing the loading of the cathode material in the battery design can be used to evaluate the influence of electrolyte on the cathode side.[1–3] Therefore, in order to further study the interphasial stability formed by the electrolytes on the surface of high voltage LCO, we adopted the low loading LCO (LCO, 2.5 mg cm^{-2}) and Li-metal sheet with conventional thickness (450 μm) in the following investigation. Figure 7b,c respectively shows the residual current at 4.6 V, and the self-discharge test of the LCO||Li cells after three cycles. Both results reveal that the interphasial stability of 3 M FMS-based electrolyte on high voltage LCO cathode is obviously better than that of carbonate-based system. It is worth mentioning that, as shown in Figure 7b, even after 20 h of constant voltage, the CBE system still shows obvious residual current, indicating that the oxidative decomposition of the electrolyte system hardly stops under the condition of high voltage. The stable CEI film formation in the 3 M FMS-based electrolyte on the surface of high-voltage LCO contributes to a capacity retention as high as 94.0% (Figure 7d) and maintains stable CE after 300 cycles (Figure 7e). In contrast, the capacity of the one with CBE drops to almost zero after only 45 cycles. Moreover, the CE of CBE system is lower than 80% during cycling (Figure 7e), which further confirms that the CBE is unstable on the surface of high-voltage LCO. The initial charge/discharge curves of the LCO||Li cell depicted in Figure 7f show that the stable CEI film formed by the 3 M FMS-based electrolyte on the LCO surface not only greatly enhances the CE of the cell, but also effectively mitigates the electrode polarization and increases the discharge capacity. It is worth noting that the initial cell capacity shown in Figure 7d increases during cycling, particularly for the electrolyte system based on carbonate. This phenomenon may be attributed to the higher salt concentration of these two electrolytes and their inferior wettability with cell materials (Figure S2, Supporting Information).

The surface morphology of the cycled LCO electrodes is shown in **Figure 8**a–f, together with the fresh LCO electrode for comparison. The SEM and TEM images of LCO after cycling with 3 M CBE clearly confirm that under high voltage conditions, CBE undergoes severe oxidative decomposition, resulting in the accumulation of a large number of decomposition products on the surface of LCO. In contrast, after cycling with the 3 M FMS-based electrolyte, a thin and homogeneous layer of electrolyte decomposition products known as CEI film is observed to cover the surface of LCO. Simultaneously, AFM characterization results indicate that the interfacial film formed by 3 M FMS-based electrolyte on the surface of L-LCO exhibits a smoother texture (Figure 8h) and more uniform composition distribution (Figure 8j) compared to that of CBE system (Figure 8g,i). Furthermore, as depicted in Figure 8k, the interphase constructed from the former exhibits significantly higher values of Young's modulus, indicating its superior robustness and stability.

The XPS characterization further confirms the thickness of the film of CBE decomposition products covering the electrode surface, as evidenced by the disappearance of M–O bond (529.5 eV in O1s) from LCO material and C–F bond (687.7 eV in F1s) from PVDF binder.[62–64] In contrast, these two peaks remain detectable even after cycling in 3 M FMS-based electrolyte, providing further confirmation that the deposition of decomposition products on the electrode surface is thinner. Note that the peak strength of the C–F bond in the 3 M FMS-based system remains unexpectedly high, potentially attributed to a portion of the C–F bond originating from FMS solvent decomposition. Furthermore, solely the Si-containing decomposition products can be detected within the 3 M FMS-based system, thereby verifying the oxidative degradation of FMS and consequent formation of the CEI film. The appearance of S=O (532.6 eV in O1s), S–F (686.5 eV in F1s), and LiF (684.8 eV in F1s) bonds in both systems suggests that the FSI^- anion also participates in the oxidation reaction and forms the interphase together with the solvent.[42–44] As shown in Figure S14d,e (Supporting Information), the CEI film formed by the 3 M FMS-based electrolyte system at LCO exhibits a higher concentration of F, N, and S elements as well as Si element compared to that formed by the 3 M EC/EMC-based system. This results in a denser and more stable CEI film with the former electrolyte system.

Dissolution of transition metal (TM) ions not only damages the structure of the cathode material, but also migrates and deposits onto the anode surface, thereby compromising its stability and ultimately leading to further deterioration in battery performances.[65–68] It has recently been reported that the absence of a stable CEI film on the surface of LCO materials results in increased formation of Co^{2+} at its interface, ultimately leading to greater dissolution and deposition onto the anode surface.[69] Therefore, to elucidate the impact of CEI film formed by the FMS-based electrolyte on Co dissolution and deposition, we conducted a series of experimental investigations. As shown in Figure S15a (Supporting Information), the Co peak on the surface of LCO was weakened after cycling in a 3 M EC/EMC-based electrolyte, with only Co^{2+} detected. This suggests severe decomposition of the carbonate-based electrolyte and significant leaching out of transition metals from the surface of LCO, resulting in decreased chemical valence. In contrast, the Co spectra of LCO remained relatively stable even after exposure to FMS-based electrolyte, which can be attributed to the formation of a robust and enduring CEI film by the electrolyte on the surface of LCO. As shown in Figure S15b–e (Supporting Information), the CEI film constructed by FMS effectively inhibits the dissolution of Co element, thereby significantly reducing the residual Co content in the electrolyte, separator, and lithium anode after cycling. The SEM images in Figure S15f (Supporting Information) reveal that the morphology of Li anode cycled in 3 M EC/EMC-based electrolyte exhibits less homogeneity compared to that in 3 M FMS-based electrolyte, indicating the superior ability of FMS system to suppress the transition metal crossover effect.

Finally, the possible SEI/CEI formation mechanism of FMS-based electrolyte is summarized in **Scheme 1**. The FMS solvent promotes the formation of Li^+-FSI^- contact ion pairs (CIPs) and cation–anion aggregates (AGGs) structure in the electrolyte, resulting in a greater number of FSI^- anions entering into the first solvation sheath compared to carbonate-based electrolytes. This

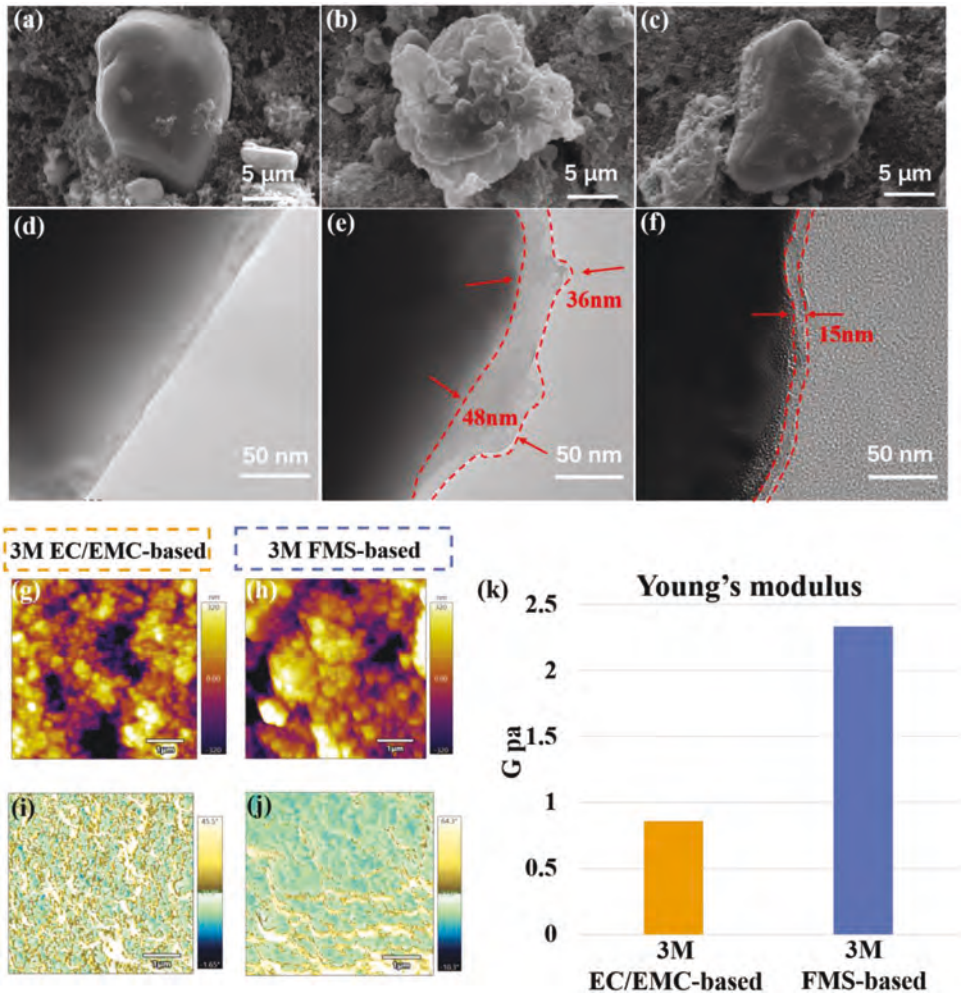

Figure 8. SEM and TEM images of fresh LCO a,d) and LCO after 10 cycles at 0.5 C in 3 M EC/EMC-based electrolyte b,e) and 3 M FMS-based electrolyte c,f). AFM surface morphology g,h), phase images i,j) and Young's modulus k) of LCO cathodes after five cycles in 3 M EC/EMC-based electrolyte and 3 M FMS-based electrolyte.

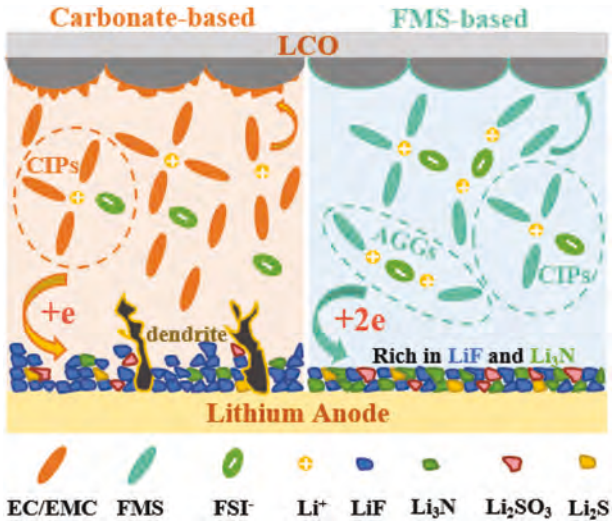

Scheme 1. Schematic diagram illustrating the possible SEI/CEI formation mechanism of FMS-based electrolytes.

improves the reduction activity of Li^+-FSI^- and lead to formation of a stable SEI film rich in LiF and Li_3N on the Li-metal surface. The oxidative decomposition of FMS solvent generates a CEI film with high oxidation resistance, thereby ensuring the long-term cycling stability of high-voltage Li-metal batteries.

3. Conclusion

In this work, we proposed a new solvent, FMS, as novel electrolyte for high voltage LMBs. The electrolyte composed of this single solvent and 3 M LiFSI (3 M FMS-based) successfully supported the long-term cycling stability of limited-Li (50 μm)||high loading LCO (≈20 mg cm^{-2}) cell at 4.6 V. The capacity retention of the cell remained at 92.5% after 100 cycles at room temperature, with the average Coulombic efficiency reached 99.5%. Under the high temperature of 60 °C, the capacity retention can be maintained at 86.7% even after 50 cycles. In contrast, in carbonates-based electrolytes at the same LiFSI concentration, the capacity of the cell decreased to 0 after less than three cycles. It is shown from experiments and theoretical simulation that the outstanding

performance of 3 M FMS-based electrolyte in high-voltage LMB is mainly due to its great ability to form a highly stable and robust interphase on the surface of lithium anode and high-voltage cathode. The FMS solvent facilitates the formation of contact ion pairs (CIPs) and cation–anion aggregates (AGGs) structures in the electrolyte. Additionally, FMS enhances the reduction activity of FSI- ions, particularly for two-electron reduction, resulting in a stable SEI film rich in LiF, Li_3N, and Li_2SO_3 on the surface of lithium metal. This inhibits dendrite growth and electrode polarization increase. On the cathode side, FMS undergoes oxidation and decomposition prior to FSI-, leading to the formation of a CEI film with superior oxidation resistance and robustness on the surface of high voltage LCO. The proposed FMS-based electrolyte not only introduces a novel design concept, but also offers a unique film-forming mechanism that has the potential to open up new avenues for the development of high-voltage LMB electrolytes.

4. Experimental Section

Electrolyte Preparations and Coin Cell Assembly: Battery-grade carbonate solvents, ethylene carbonate (EC), ethyl methyl carbonate (EMC), and lithium bisfluorosulfonimide (LiFSI) were provided by Guangzhou Tinci Material Technology Co., Ltd. TFPMDS solvent was purchased from TCI. All chemicals were used without further purification. A carbonate-based electrolyte consisting of 1 M LiFSI in EC/EMC (3/7, vol) and 3 M LiFSI in EC/EMC (3/7, vol) was used as reference. Dissolve 1 M LiFSI in FMS solvent to form the 1 M FMS-based electrolyte. Dissolve 3 M LiFSI in FMS solvent to form the 3 M FMS-based electrolyte. All electrolytes were prepared in an argon-filled glove box (MBraun, Germany). Cathode material particle slurry (LCO, Guangzhou Penghui Energy Technology Co., Ltd.), polyvinylidene fluoride (PVDF), Super-P binder (96.8:1.2:2), weight ratio) in N-methylpyrrolidone (NMP) solvent, the mixture was coated on aluminum foil, then vacuum-dried at 80 °C for 1 h, 120 °C for 12 h, and finally cut into 1.13 cm^{-2} to prepare LCO electrodes. The areal mass loading of the high-load LCO (H-LCO) is about 20 mg cm^{-2}. The areal mass loading of a low-load LCO (LCO) is approximately 2.5 mg cm^{-2}. Battery-grade thick lithium foil (Li, diameter = 15.6 mm, thickness = 450 μm) and battery-grade thin lithium foil (L-Li, thickness = 50 μm) were purchased from China Energy Lithium Co., Ltd. CR2025 coin-type cells were assembled with Celgard 2400 separator and different electrolytes in the argon-filled glove box (H_2O, O_2 < 1 ppm), and the amount of electrolyte is controlled at 60 μL in all coin cells.

Electrochemical Tests: The charge/discharge tests were conducted on LAND cell test system (Land CT 2000 China). The Li//Li symmetric cells were tested at different densities (1.0 and 2.0 mA cm^{-2}) for Li striping/depositing in various electrolytes. The Li//Cu cells were cycled at different current densities (1.0, 2.0 mA cm^{-2}). In each cycle, the cells were first discharged for 1.0 h, and then charged to the cutoff voltage of 1 V. The Li//Li and Li//Cu rate performance tests were performed by cycling at various current densities (j = 0.2, 0.5, 1, 2, and 3 mA cm^{-2} for five times each in turn, and then back to 0.2 mA cm^{-2}). The H-LCO||L-Li cells were cycled in the potential range of 3–4.6 V (vs Li/Li^+) at 0.2 C (1 C = 190 mA h g^{-1}) in various electrolytes. The H-LCO||L-Li cells were also cycled in the potential range of 3–4.6 V (vs Li/Li^+) at 0.2 C in various electrolytes under 60 °C. The LCO||Li cells were cycled in the potential range of 3–4.6 V (vs Li/Li^+) at 0.5 C (1 C = 190 mA h g^{-1}) in various electrolytes. Various electrolytes were measured by linear sweep voltammetry (LSV) in the voltage range of 3–5 V (vs Li/Li^+) at a scan rate of 0.1 mV s^{-1} on a Solartron-1470 instrument in the UK by using Li||Pt cells. Linear scanning voltammetry (LSV) measurements of various electrolytes were performed at a scan rate of 0.1 mV s^{-1} over the voltage range of 3–4.6 V (vs Li/Li^+) on a Solartron-1480 (England) using Li||LCO V-type cells, followed by a constant voltage of 4.6 V for 12 h to observe the liquid level difference of the V-type cells. Chronoamperometry (CA) was scanned three times at a scan rate of 0.5 mV s^{-1} over a voltage range of 3–4.6 V (vs Li/Li^+) on a Solartron-1480 (England) and then held at a constant voltage of 4.6 V for 20 h to record the change in current. Self-discharge profiles cells cycled 3 times between 3 and 4.6 V at 0.5C and charged to 4.6 V and then left to stand and the voltage change were recorded. Electrochemical impedance spectroscopy (EIS) of LCO/Li cells after one and three cycles with different electrolytes were tested separately on a PGSTAT-30 electrochemical station (Autolab, Switzerland).

Online O_2, CO_2, and SO_2 evolution was performed on an HPR-40 DEMS mass spectrometer system (HIDEN Analytical, UK) and an ECC air cell (EL-cell, Germany), where 15.6 mm∅ lithium foil, PP separator, 40 μL electrolyte and cathode (LCO, 2.5 mg cm^{-2}) were added sequentially. The cell was degassed for 2 h under continuous Ar flow (0.5 mL min^{-1}) to remove residual gas prior to measurement. In addition, to minimize the detection delay, the Ar gas flow was also passed through the cell during the measurement.

Physical Characterization: The cycled Li//Li and Li//Cu cells were disassembled within the argon-filled glove box and Li electrode (Cu electrode) was recovered, followed by laundry thrice with EMC solvent to get rid of the residual solution. The morphologies of Li electrode and LCO electrode surface were observed with scanning electron microscope (FEI-SEM, FEI-Quanta-250, America). The solvated structural changes at different salt concentrations using in 532 nm wavelength laser obtain to Raman spectra (WITec Alpha 300R, alpha 300, Germany). Transmission electron microscopy (TEM, JEM-2100, JOEL, Japan) were used to observe the surface morphology and particle integrity of the LCO electrode and Li electrode. Operando optical microscopy(YM710TR, China) images of lithium anodes cycled in various electrolytes in a transparent cell with a fixed current density of 1 mA cm^{-2}. The compositions of surface film on the Li-metal anode and LCO electrode before and after cycling were analyzed by X-ray photoelectron spectroscopy (XPS) using an ESCALAB 250 X-ray photoelectron spectrometer (Thermo Fisher Scientific, America). The depth profiles were obtained via Ar^+ sputtering at 1 kV for 0, 1, 2, and 4 min. The mass contents of the elements were obtained from the XPS fitting. The ionic conductivity of electrolytes was tested by the 856 Conductivity Module (Metrohm, Switzerland). The solvated structural changes at different salt concentrations were measured with FTIR (Bruker Tensor 27, Germany). The content of transition metal ions dissolved in different electrolytes after 10 cycles in V-type cells and the content of transition metals deposited in lithium electrodes and separators after 10 cycles in LCO/Li coin cells were determined by inductively coupled plasma (ICP)-atomic emission spectrometry. The contact angles between separator and electrolytes were measured using a contact angle meter (JC 2000D3P, Shanghai). The viscosity of various electrolytes was measured by viscometer (Anton Paar Lovis 2000 M). The surface flatness and mechanical strength of the LCO electrode before and after the cycle were tested by Atomic force microscope (AFM, Oxford MFP-3D Origin).

Supporting Information

Supporting Information is available from the Wiley Online Library or from the author.

Acknowledgements

Y.L. and M.L. contributed equally to this work. This work was supported by the National Natural Science Foundation of China (Grant No. 22179041) and US National Science Foundation (Grant No. 2211825).

Conflict of Interest

The authors declare no conflict of interest.

Data Availability Statement

Research data are not shared.

Keywords

high-voltage applications, inorganic interfaces, lithium-metal batteries, Li^+ solvation, siloxanes

Received: March 26, 2023
Revised: June 8, 2023
Published online:

[1] X. R. Chen, B. C. Zhao, C. Yan, Q. Zhang, *Adv. Mater.* **2021**, *33*, 2004128.
[2] Y. Jie, X. Ren, R. Cao, W. Cai, S. Jiao, *Adv. Funct. Mater.* **2020**, *30*, 1910777.
[3] H. Wang, Z. Yu, X. Kong, S. C. Kim, D. T. Boyle, J. Qin, Y. Cui, *Joule* **2022**, *3*, 588.
[4] D. Lu, X. C. Lei, S. T. Weng, R. H. Li, J. D. Li, L. Lv, H. K. Zhang, Y. Q. Huang, J. B. Zhang, S. Q. Zhang, L. W. Fan, X. F. Wang, L. X. Chen, G. L. Cui, D. Su, X. L. Fan, *Energy Environ. Sci.* **2022**, *15*, 3331.
[5] Y. Huang, R. Li, S. Weng, H. Zhang, C. Zhu, D. Lu, C. Sun, X. Huang, T. Deng, L. Fan, L. Chen, X. Wang, X. Fan, *Energy Environ. Sci.* **2022**, *15*, 4349.
[6] H. Wang, Y. Liu, Y. Li, Y. Cui, *Electrochem. Energy Rev.* **2019**, *2*, 509.
[7] Q. Zhang, S. Liu, Y. Lu, L. Xing, W. Li, *J. Energy Chem.* **2021**, *58*, 198.
[8] A. C. Thenuwara, P. P. Shetty, N. Kondekar, S. E. Sandoval, K. Cavallaro, R. May, C.-T. Yang, L. E. Marbella, Y. Qi, M. T. McDowell, *ACS Energy Lett.* **2020**, *5*, 2411.
[9] S. Zhang, G. Yang, Z. Liu, X. Li, X. Wang, R. Chen, F. Wu, Z. Wang, L. Chen, *Nano Lett.* **2021**, *21*, 3310.
[10] X. S. Wang, S. W. Wang, H. R. Wang, W. Q. Tu, Y. Zhao, S. Li, Q. Liu, J. R. Wu, Y. Z. Fu, C. P. Han, F. Y. Kang, B. H. Li, *Adv. Mater.* **2021**, *33*, 2007945.
[11] H. Ye, Y. Zhang, Y.-X. Yin, F.-F. Cao, Y.-G. Guo, *ACS Cent Sci* **2020**, *6*, 661.
[12] L. Xiao, Z. Zeng, X. Liu, Y. Fang, X. Jiang, Y. Shao, L. Zhuang, X. Ai, H. Yang, Y. Cao, J. Liu, *ACS Energy Lett.* **2019**, *4*, 483.
[13] Q. K. Zhang, X. Q. Zhang, L. P. Hou, S. Y. Sun, Y. X. Zhan, J. L. Liang, F. S. Zhang, X. N. Feng, B. Q. Li, J. Q. Huang, *Adv. Energy Mater.* **2022**, *12*, 2200139.
[14] Y. Fan, T. Tao, Y. Gao, C. Deng, B. Yu, Y. I. Chen, S. Lu, S. Huang, *Adv. Mater.* **2020**, *32*, 2004798.
[15] Y. C. Yin, Q. Wang, J. T. Yang, F. Li, G. Zhang, C. H. Jiang, H. S. Mo, J. S. Yao, K. H. Wang, F. Zhou, H. X. Ju, H. B. Yao, *Nat. Commun.* **2020**, *11*, 1761.
[16] F. Q. Liu, W. P. Wang, Y. X. Yin, S. F. Zhang, J. L. Shi, L. Wang, X. D. Zhang, Y. Zheng, J. J. Zhou, L. Li, Y. G. Guo, *Sci. Adv.* **2018**, *4*, eaat5383.
[17] H. Zhang, Z. Zeng, R. He, Y. Wu, W. Hu, S. Lei, M. Liu, S. Cheng, J. Xie, *Energy Storage Mater.* **2022**, *48*, 393.
[18] L. J. Tan, S. Q. Chen, Y. W. Chen, J. J. Fan, D. G. Ruan, Q. S. Nian, L. Chen, S. H. Jiao, X. D. Ren, *Angew. Chem., Int. Ed.* **2022**, *61*, 202203693.
[19] H. Wang, Z. Yu, X. Kong, W. Huang, Z. Zhang, D. G. Mackanic, X. Huang, J. Qin, Z. Bao, Y. Cui, *Adv. Mater.* **2021**, *33*, 2008619.
[20] J. Fu, X. Ji, J. Chen, L. Chen, X. Fan, D. Mu, C. Wang, *Angew. Chem., Int. Ed.* **2020**, *59*, 22378.
[21] Z. Jiang, Z. Zeng, X. Liang, L. Yang, W. Hu, C. Zhang, Z. Han, J. Feng, J. Xie, *Adv. Funct. Mater.* **2021**, *31*, 2005991.
[22] Q. Zhao, X. Liu, J. Zheng, Y. Deng, A. Warren, Q. Zhang, L. Archer, *Proc. Natl. Acad. Sci. U. S. A.* **2020**, *117*, 26053.
[23] H. Zhang, Z. Q. Zeng, F. F. Ma, Q. Wu, X. L. Wang, S. J. Cheng, J. Xie, *Angew. Chem., Int. Ed.* **2023**, 202300771.
[24] K. Xu, *Chem. Rev.* **2014**, *114*, 11503.
[25] T. Z. Hou, X. Chen, L. Jiang, C. Tang, *Int. J. Electrochem.* **2022**, *28*, 2219007.
[26] J. Y. Wang, S. N. Guo, X. Wang, L. Gu, D. Su, *Int. J. Electrochem.* **2022**, *28*, 2108431.
[27] X. Zheng, L. Huang, X. Ye, J. Zhang, F. Min, W. Luo, Y. Huang, *Chem* **2021**, *7*, 2312.
[28] H. Wang, J. Song, K. Zhang, Q. Fang, Y. Zuo, T. Yang, Y. Yang, C. Gao, X. Wang, Q. Pang, D. Xia, *Energy Environ. Sci.* **2022**, *15*, 5149.
[29] Q. K. Zhang, X.-Q. Zhang, H. Yuan, J.-Q. Huang, *Small Sci.* **2021**, *1*, 2100058.
[30] H. Liang, X. Zuo, L. Zhang, W. Huang, Q. Chen, T. Zhu, J. Liu, J. Nan, *J. Electrochem. Soc.* **2020**, *167*, 090520.
[31] J. Zheng, X. Fan, G. Ji, H. Wang, S. Hou, K. C. DeMella, S. R. Raghavan, J. Wang, K. Xu, C. Wang, *Nano Energy* **2018**, *50*, 431.
[32] B. Horstmann, J. Shi, R. Amine, M. Werres, X. He, H. Jia, F. Hausen, I. Cekic-Laskovic, S. Wiemers-Meyer, J. Lopez, D. Galvez-Aranda, F. Baakes, D. Bresser, C.-C. Su, Y. Xu, W. Xu, P. Jakes, R.-A. Eichel, E. Figgemeier, U. Krewer, J. M. Seminario, P. B. Balbuena, C. Wang, S. Passerini, Y. Shao-Horn, M. Winter, K. Amine, R. Kostecki, A. Latz, *Energy Environ. Sci.* **2021**, *14*, 5289.
[33] C. X. Zhang, Z. Lu, M. Song, Y. Q. Zhang, C. Y. Jing, L. B. Chen, X. B. Ji, W. F. Wei, *Adv. Energy Mater.* **2023**, *13*, 2203870.
[34] Z. C. Wang, H. Y. Zhang, J. J. Xu, A. R. Pan, F. R. Zhang, L. Wang, R. Han, J. C. Hu, M. N. Liu, X. D. Wu, *Adv. Funct. Mater.* **2022**, *32*, 2112598.
[35] W. N. Zhang, T. Yang, X. B. Liao, Y. Song, Y. Zhao, *Energy Storage Mater.* **2023**, *57*, 249.
[36] D. G. Ruan, L. J. Tan, S. Q. Chen, J. J. Fan, Q. S. Nian, L. Chen, Z. H. Wang, X. D. Ren, *Jacs Au* **2023**, *3*, 953.
[37] Z. Peng, X. Cao, P. Gao, H. Jia, X. Ren, S. Roy, Z. Li, Y. Zhu, W. Xie, D. Liu, Q. Li, D. Wang, W. Xu, J.-G. Zhang, *Adv. Funct. Mater.* **2020**, *30*, 2001285.
[38] J. Fu, X. Ji, J. Chen, L. Chen, X. Fan, D. Mu, C. Wang, *Angew. Chem., Int. Ed.* **2020**, *59*, 22194.
[39] X. Ren, L. Zou, S. Jiao, D. Mei, M. H. Engelhard, Q. Li, H. Lee, C. Niu, B. D. Adams, C. Wang, J. Liu, J.-G. Zhang, W. Xu, *ACS Energy Lett.* **2019**, *4*, 896.
[40] Z. Zeng, V. Murugesan, K. S. Han, X. Jiang, Y. Cao, L. Xiao, X. Ai, H. Yang, J. G. Zhang, M. L. Sushko, J. Liu, *Nat. Energy* **2018**, *3*, 674.
[41] Y. X. Yao, X. Chen, C. Yan, X. Q. Zhang, W. L. Cai, J. Q. Huang, Q. Zhang, *Angew. Chem., Int. Ed.* **2021**, *60*, 4090.
[42] T. Li, X. Zhang, N. Yao, Y. Yao, L. Hou, X. Chen, M. Zhou, J. Huang, Q. Zhang, *Angew. Chem., Int. Ed.* **2021**, *60*, 22683.
[43] J. F. Ding, R. Xu, N. Yao, X. Chen, Y. Xiao, Y. X. Yao, C. Yan, J. Xie, J. Q. Huang, *Angew. Chem., Int. Ed.* **2021**, *60*, 11442.
[44] Z. Chang, Y. Qiao, H. Deng, H. Yang, P. He, H. Zhou, *Energy Environ. Sci.* **2020**, *13*, 1197.
[45] T. D. Pham, A. Bin Faheem, J. Kim, H. M. Oh, K. K. Lee, *Small* **2022**, *18*, 2107492.
[46] S. Chen, J. Zheng, L. Yu, X. Ren, M. H. Engelhard, C. Niu, H. Lee, W. Xu, J. Xiao, J. Liu, J.-G. Zhang, *Joule* **2018**, *2*, 1548.
[47] X. Fan, X. Ji, L. Chen, J. Chen, T. Deng, F. Han, J. Yue, N. Piao, R. Wang, X. Zhou, X. Xiao, L. Chen, C. Wang, *Nat. Energy* **2019**, *4*, 882.
[48] X. Ren, S. Chen, H. Lee, D. Mei, M. H. Engelhard, S. D. Burton, W. Zhao, J. Zheng, Q. Li, M. S. Ding, M. Schroeder, J. Alvarado, K. Xu, Y. S. Meng, J. Liu, J.-G. Zhang, W. Xu, *Chem* **2018**, *4*, 1877.
[49] C. Zhu, C. Sun, R. Li, S. Weng, L. Fan, X. Wang, L. Chen, M. Noked, X. Fan, *ACS Energy Lett.* **2022**, *7*, 1338.
[50] X. Zheng, Z. Gu, X. Liu, Z. Wang, J. Wen, X. Wu, W. Luo, Y. Huang, *Energy Environ. Sci.* **2020**, *13*, 1788.
[51] X. Zheng, L. Huang, W. Luo, H. Wang, Y. Dai, X. Liu, Z. Wang, H. Zheng, Y. Huang, *ACS Energy Lett.* **2021**, *6*, 2054.
[52] C. Jin, T. Liu, O. Sheng, M. Li, T. Liu, Y. Yuan, J. Nai, Z. Ju, W. Zhang, Y. Liu, *Nat. Energy* **2021**, *6*, 378.

[53] R. Amine, J. Z. Liu, I. Acznik, T. Sheng, K. Lota, H. Sun, C. J. Sun, K. Fic, X. B. Zuo, Y. Ren, D. Abd El-Hady, W. Alshitari, A. S. Al-Bogami, Z. H. Chen, K. Amine, G. L. Xu, *Adv. Energy Mater.* **2020**, *10*, 2000901.
[54] X. Q. Zhang, X. Chen, L. P. Hou, B. Q. Li, X. B. Cheng, J. Q. Huang, Q. Zhang, *ACS Energy Lett.* **2019**, *4*, 411.
[55] T. Liu, Z. Shi, H. Li, W. Xue, S. Liu, J. Yue, M. Mao, Y.-S. Hu, H. Li, X. Huang, L. Chen, L. Suo, *Adv. Mater.* **2021**, *33*, 2102034.
[56] S. Liu, X. Ji, N. Piao, J. Chen, N. Eidson, J. Xu, P. Wang, L. Chen, J. Zhang, T. Deng, S. Hou, T. Jin, H. Wan, J. Li, J. Tu, C. Wang, *Angew. Chem., Int. Ed.* **2021**, *60*, 3661.
[57] C. Liao, L. Han, W. Wang, W. Li, X. Mu, Y. Kan, J. Zhu, Z. Gui, X. He, L. Song, Y. Hu, *Adv. Funct. Mater.* **2023**, *17*, 2212605.
[58] X. Q. Zhang, X. Chen, X. B. Cheng, B. Q. Li, X. Shen, C. Yan, J. Q. Huang, Q. Zhang, *Angew. Chem., Int. Ed.* **2018**, *57*, 5301.
[59] S. Li, W. Zhang, Q. Wu, L. Fan, Y. Lu, *Angew. Chem., Int. Ed.* **2020**, *59*, 14935.
[60] S. H. Lee, J. Y. Hwang, J. Ming, Z. Cao, H. A. Nguyen, H. G. Jung, J. Kim, Y. K. Sun, *Adv. Energy Mater.* **2020**, *10*, 2000567.
[61] J.-Y. Wei, X.-Q. Zhang, L.-P. Hou, P. Shi, B.-Q. Li, Y. Xiao, C. Yan, H. Yuan, J.-Q. Huang, *Adv. Mater.* **2020**, *32*, 2003012.
[62] D. Ruan, M. Chen, X. Wen, S. Li, X. Zhou, Y. Che, J. Chen, W. Xiang, S. Li, H. Wang, X. Liu, W. Li, *Nano Energy* **2021**, *90*, 106535.
[63] B. Liao, H. Li, M. Xu, L. Xing, Y. Liao, X. Ren, W. Fan, L. Yu, K. Xu, W. Li, *Adv. Energy Mater.* **2018**, *8*, 1800802.
[64] Y. Che, X. Lin, L. Xing, X. Guan, R. Guo, G. Lan, Q. Zheng, W. Zhang, W. Li, *J. Energy Chem* **2021**, *52*, 361.
[65] J. Langdon, A. Manthiram, *Adv. Mater.* **2022**, *34*, 2205188.
[66] J. Wandt, A. Freiberg, R. Thomas, Y. Gorlin, A. Siebel, R. Jung, H. A. Gasteiger, M. Tromp, *J. Mater. Chem. A* **2016**, *4*, 18300.
[67] S. Solchenbach, G. Hong, A. Teresa, S. Freiberg, R. Jung, H. A. Gasteiger, *J. Electrochem. Soc.* **2018**, *165*, A3304.
[68] H. Y. Xu, Z. P. Li, T. C. Liu, C. Han, C. Guo, H. Zhao, Q. Li, J. Lu, K. Amine, X. P. Qiu, *Angew. Chem., Int. Ed.* **2021**, *30*, 202202894.
[69] S. Tan, Z. Shadike, J. Z. Li, X. L. Wang, Y. Yang, R. Q. Lin, A. Cresce, J. T. Hu, A. Hunt, I. Waluyo, L. Ma, F. Monaco, P. Cloetens, J. Xiao, Y. J. Liu, X. Q. Yang, K. Xu, E. Y. Hu, *Nat. Energy* **2022**, *7*, 484.